Applied Physics A (2026) 132:482
https://doi.org/10.1007/s00339-026-09664-2

Applied Physics A
Materials Science & Processing

Intraband absorption in the Deng-Fan type quantum well under magnetic field and hydrostatic pressure: comparison with the Morse quantum well

Esin Kasapoglu[1] · **Melike Behiye Yücel**[2]

Received: 5 February 2026 / Accepted: 28 April 2026
© The Author(s) 2026

Abstract

This work explores how the magnetic field, hydrostatic pressure, and well dimensions affect the electronic and optical properties of a quantum well with a Deng-Fan molecular potential. The calculations were performed within the effective mass and parabolic band approximation frameworks. These investigations have involved analyzing the energy spectrum and determining both the linear and third-order nonlinear absorption coefficients. To solve the Schrödinger equation of the system, the diagonalization method was utilized by choosing orthonormal base functions. For the absorption coefficients, the standard density matrix formalism combined with the perturbation expansion method is used. Our calculations were extended to include the traditional Morse-type quantum well. It is observed that the peak positions of the total absorption coefficients associated with the (1–2) intraband transitions in the Morse quantum well are located at relatively low photon energies, which can be attributed to the weak geometric confinement of the potential. In contrast, for equivalent quantum well widths, the Deng–Fan potential yields larger transition energies and higher peak amplitudes. This enhancement arises from its stronger effective confinement and improved short-range behavior. Moreover, the Deng–Fan potential provides superior tunability of potential asymmetry, allowing more precise control over the electronic structure and optical response.

Keywords Deng-Fan potential · Morse potential · Quantum well · Magnetic field · Hydrostatic pressure · Intraband absorption

1 Introduction

When working with the quantum wells, wires, and dots, choosing the most appropriate potential is an important step, especially for the development of optoelectronic devices. In addition to the selection of confinement potential, the effects of the electric field, magnetic field, and intense laser fields, temperature, and hydrostatic pressure are powerful tools to control the electrical and optical responses of the semiconductor heterostructures. Since these properties can be altered according to the purposes, studying the effects of applied external fields and potential geometries on charge carriers confined in any quantum system has become the most important area of research. Researchers have focused on understanding how these external fields influence phenomena such as quantum confinement, bandgap tuning, and exciton dynamics. As a result, the exploration of these effects not only enhances the fundamental understanding of low-dimensional systems but also opens new avenues for innovative applications in next-generation optoelectronic devices.

With technological progress, it has become feasible to fabricate low-dimensional semiconductor systems in various shapes and sizes. This is because traditional potential models like rectangular or parabolic wells fail to accurately capture the atomic-scale characteristics of materials [1–12].

✉ Esin Kasapoglu
ekasap@cumhuriyet.edu.tr

Melike Behiye Yücel
myucel@akdeniz.edu.tr

[1] Physics Department, Sivas Cumhuriyet University Science Faculty, 58140 Sivas, Türkiye

[2] Science Faculty, Physics Department, Akdeniz University, 07058 Antalya, Türkiye

Published online: 11 May 2026

Recently, extensive research has focused on the quantum structures modeled by molecular potentials such as Morse [13], Tietz-Hua [14], Konwent [15], Manning [16], Rosen-Morse [17], and Razavy potentials [18, 19]. Molecular potentials are considered to be more realistic and better aligned with experimental observations. In the present study, the Deng–Fan potential also known as the generalized Morse potential, originally introduced by Deng and Fan to describe the vibrational spectra of diatomic molecules [20], this potential exhibits improved asymptotic behavior as the spatial coordinate approaches zero when compared to the conventional Morse potential. Such behavior makes the Deng–Fan potential particularly attractive for modeling low-dimensional semiconductor systems. It should also be noted that two potentials will be compared for the same material parameters in this study.

One of its key features is its inherently asymmetric confinement profile. Unlike symmetric model potentials, the Deng–Fan potential naturally represents quantum wells (QWs) with unequal barrier heights on opposite sides, closely resembling realistic semiconductor heterostructures with graded compositions or asymmetric interfaces. In addition, its exponential functional form ensures smooth and physically realistic potential transitions, avoiding the abrupt discontinuities characteristic of rectangular quantum wells. The improved short-range behavior of the Deng–Fan potential further enhances its suitability for narrow QWs, where interface effects and strong confinement play a dominant role.

Despite its significant advantages, the Deng–Fan potential has received limited attention in semiconductor nanostructure research. To the best of our knowledge, it has only been applied to spherical quantum dots in combination with Eckart-type potentials [21–23]. However, very recently, the effects of magnetic and intense laser fields on the electronic and optical properties of a shifted Deng–Fan type QW, and the effects of hydrostatic pressure on the electronic and optical properties of isotropic and anisotropic two-dimensional quantum dots with the Deng–Fan oscillator potential were investigated in Refs [24, 25]., respectively.

External fields, such as the magnetic fields and the hydrostatic pressure, constitute powerful experimental tools for tuning the electronic and optical properties of semiconductor heterostructures. A magnetic field quantizes the in-plane carrier motion and modifies the confinement energy, while the hydrostatic pressure simultaneously affects several material parameters, including the effective mass, band-gap energy, dielectric constant, and geometric dimensions through elastic compression. A comprehensive understanding of how these external probes interact with different confinement geometries is therefore crucial for the design and optimization of tunable optoelectronic devices. The primary objective of this study is to examine the influence of the magnetic field strength, the hydrostatic pressure, and structural parameters on the electronic energy spectrum and intraband transition properties of electrons confined in a quantum well (QW) modeled by the Deng–Fan potential. The organization of the paper is as follows. Section 2 presents the theoretical model and formalism. The numerical results and their detailed discussion are provided in Sect. 3. Finally, Sect. 4 summarizes the main findings and conclusions of the study.

2 Theory

In the effective mass approximation, the Hamiltonian for an electron confined within the QW in the presence of the hydrostatic pressure and the magnetic field is as follows

$$H = \frac{1}{2m^*(P)}\left[\vec{p} + \frac{e}{c}\vec{A}(\vec{r})\right]^2 + V(z,P) \tag{1}$$

where $m^*(P)$ and $\vec{p}$ are the pressure dependent effective mass and momentum of the electron, $\vec{A}(\vec{r})$ is the vector potential. The magnetic field is applied perpendicular to the growth direction (z-direction), i.e. $\vec{B} = (0, B, 0)$ is the magnetic field strength, in the Landau gauge ($\vec{B} = \vec{\nabla} x \vec{A}$), the vector potential associated to the applied magnetic field is given by $\vec{A}(\vec{r}) = (Bz, 0, 0)$, e is the elementary charge, c is the speed of light. $V(z, P)$ is the confinement potential.

The electron wave function corresponding to the Hamiltonian in Eq. (1) can be written as [26]

$$\Phi(\vec{r}, P) = e^{-\vec{k}_\perp \vec{\rho}}\varphi(z,P) \tag{2}$$

where $\vec{k}_\perp = (k_x, k_y)$, $\vec{\rho}(x, y)$, and $\varphi(z,P)$ satisfies the following Eq.

$$\begin{aligned}&\left\{\frac{1}{2m^*(P)}\left[-\hbar^2\frac{d^2}{dz^2} + \left(\frac{eB}{c}\right)^2\left(z + \frac{c\hbar k_x}{eB}\right)^2\right] + V(z,P)\right\}\\ &\varphi(z,P) = \left[E_z - \frac{\hbar^2 k_y^2}{2m^*(P)}\right]\varphi(z,P).\end{aligned} \tag{3}$$

Since we are interested in the minimum value of the electron subbands,

$$\left[-\frac{\hbar^2}{2m^*(P)}\frac{d^2}{dz^2} + \frac{e^2B^2}{2m^*(P)c^2}z^2 + V(z,P)\right]\varphi(z,P) = E_z\varphi(z,P). \tag{4}$$

$\vec{k}_\perp = (k_x, k_y) = (0,0)$ is chosen, and as a result, Eq. (3) takes the following form

To solve the 1D Schrödinger equation, the diagonalization technique is employed by selecting orthonormal basis functions that correspond to the solutions of an infinite QW

with a width of L_b. This method requires embedding any well potential into an infinite square well, where the presence of the confining walls does not affect on the solutions. The width of the infinite square well is choosen to be large enough to ensure that the solutions are not sensitive to infinite walls, the L_b value is determined according to the convergence of the energy eigenvalues.

$\varphi\ (z, P)$-wave function is expanded in terms of a complete set of orthonormal functions [9]:

$$\varphi\ (z, P) = \sum_{n=1}^{N} c_n \psi_{\ n}\,(z, P)\,, \tag{5}$$

were N represents the matrix size. The complete set of functions is found from the analytical solution of the 1D infinite QW which has width- L_b, and is given by the following form

$$\begin{aligned} &\psi_n\,(z,\ P) = \sqrt{\tfrac{2}{L_b(P)}} cos\left(\tfrac{n\pi\, z}{L_b(P)} - \delta_n\right), \\ &\text{and } \delta_{\ n} = \begin{cases} 0, & n\ is\ odd \\ \frac{\pi}{2}, & n\ is\ even. \end{cases} \end{aligned} \tag{6}$$

The width of the QW is chosen to be sufficiently large to ensure that the obtained solutions are not affected by boundary conditions. Additionally, the matrix dimension- N is systematically increased until the results reach the desired convergence and accuracy. N and L_b must be sufficiently large to meet the convergence criteria for energy; in this study, this criterion is set at 0.1 meV for the four lowest bound states.

The hydrostatic pressure dependent effective mass for the electron is given by [27–29]

$$m^*\,(P) = \frac{m_0}{1 + E_p^{\Gamma}\left[\frac{2}{E_{\rm g}^{\Gamma}\,(P)} + \frac{1}{E_{\rm g}^{\Gamma}\,(P) + \Delta_{\,0}}\right]} \tag{7}$$

where $m^*\,(0) = 0.067 m_o$, m_0 is the free electron mass, $E_p^{\Gamma} = 7.51$ eV is energy related to the momentum matrix element for $T = 0.0$, $\Delta_{\,0} = 0.341$ eV is spin-orbit splitting and $E_{\rm g}^{\Gamma}\ (P)$ is the hydrostatic pressure dependent energy gap in the units of kbar for the GaAs quantum well at the Γ-point in the units of eV. It is given by [27–29]

$$E_{\rm g}^{\Gamma}\,(P) = 1.425 + 1.26 \times 10^{-2} P - 3.77 \times 10^{-5} P^2 \tag{8}$$

The hydrostatic pressure dependent static dielectric constant is given by [30]

$$\epsilon\ (P) = \epsilon\ (0)\ e^{\delta\, P} \tag{9}$$

where $\epsilon\ (0) = 12.58$ is dielectric constant at the atmospheric hydrostatic pressure, and $\delta = -1.73 \times 10^{-3} kbar^{-1}$. The electron is confined within a Deng-Fan type potential, the modified form of this potential, as defined in Ref [31]., and its pressure-dependent expression are given as follows

$$V\,(z, P) = V_0\,(P)\left(\frac{1 - e^{-z/L(P)}}{1 - e^{-z_o\,(P)/L(P)}}\right)^2 \tag{10}$$

where $V_o\ (P)$ is the potential depth, and is given by [30]

$$V_0\,(P) = Q_c\ \Delta\, E_{\rm g}^{\Gamma}\ (x_{Al}, P) \tag{11}$$

where $Q_c\,(= 0.6)$ is the conduction band offset parameter (in our calculations, $V_0\,(0) = 228\, meV$ corresponds to a fixed concentration $x_{Al} = 0.3$), where x_{Al} is the mole fraction of aluminum in $Ga_{1-x}Al_xAs$ layer, and $\Delta\, E_g^{\Gamma}\ (x, P)$ is the hydrostatic pressure dependent band gap difference between the QW and the barrier matrix at the Γ-point, and it is given by

$$\Delta\, E_g^{\Gamma}\ (x_{Al}, P) = 1.155\, x_{Al} + 0.37\, x_{Al}^2 - 1.3 \times\ 10^{-3} P, \tag{12}$$

In Eq. (10), $L\,(P)$ is the pressure dependent well width, and it is as follows

$$L\,(P) = L\,(0)\,(1 - (S_{11} + 2S_{12})\,P) \tag{13}$$

where $L\,(0)$ is the original well width in the absence of the hydrostatic pressure (and also z_o is the width parameter, its dependence on pressure is as in Eq. (13)), $S_{11} = 1.16x10^{-3} kbar^{-1}$ and $S_{12} = -3.7x10^{-4} kbar^{-1}$ are the elastic constants for GaAs material [27].

Using the eigenvalues and eigenfunctions derived from the solution of the Schrödinger equation, the linear, third-order nonlinear, and total absorption coefficients corresponding to transitions between arbitrary electronic states are computed through perturbation theory and the density matrix formalism [9, 16], respectively

$$\beta^{\,(1)}\,(\omega\,) = \sqrt{\frac{\mu_{\,0}}{\epsilon_r}}\frac{|M_{ij}|^2 \sigma_{\,v} \hbar\omega\, \Gamma_{\,ij}}{(E_{ij} - \hbar\omega\,)^2 + (\hbar\Gamma_{\,ij})^2} \tag{14}$$

$$\beta^{\,(3)}\,(\omega\,, I) = -2\sqrt{\tfrac{\mu_{\,0}}{\epsilon_r}}\left(\tfrac{I}{\epsilon_{\,0} n_r c}\right)\tfrac{|M_{ij}|^2 \sigma_{\,v} \hbar\omega\, \Gamma_{\,ij}}{(E_{ij} - \hbar\omega\,)^2 + (\hbar\Gamma_{\,ij})^2} \left(1 - \tfrac{|M_{jj} - M_{ii}|^2}{|2M_{ij}|^2}\tfrac{(E_{ij} - \hbar\omega\,)^2 - (\hbar\Gamma_{ij})^2 + E_{ij}(E_{ij} - \hbar\omega)}{E_{ij}^2 + (\hbar\Gamma_{\,ij})^2}\right) \tag{15}$$

$$\beta\,(\omega\,, I) = \beta^{\,(1)}\,(\omega\,) + \beta^{\,(3)}(\omega\,, I) \tag{16}$$

where, $\epsilon_r = n_r^2 \epsilon_{\,0}$ is the real part of the permittivity, n_r is the refractive index, $\epsilon_{\,0}$ is the permittivity of free space, $\sigma_{\,v}$ is the carrier density, $\mu_{\,0}$ is the vacuum permeability, $E_{12} = E_2 - E_1$ is the energy

difference between two energy levels of the electron, $M_{ij} = |\langle \psi_i \mid ez \mid \psi_j \rangle|$, $(i, j = 1, 2)$ is the transition matrix element between the eigenstates $\psi_i(z)$ and $\psi_j(z)$ for the light polarized in the z-direction, The relaxation rate $\Gamma_{ij} = 1/T_{ij}$ is inversely proportional to the relaxation time (T_{ij}), and I is the intensity of incident photon with the ω -angular frequency that provides intraband transitions.

3 Results and discussions

The values of the parameters in our calculations are $\varepsilon_0 = 8.85 \times 10^{-12} C^2 N^{-1} m^{-2}$, $n_r = 3.55$, $T_{12} = 0.4\, ps$, $\mu_o = 4\pi \times 10^{-7} Hm^{-1}$, $\sigma_v = 3.0 \times 10^{22}\, e/m^3$ and $I = 5.0 \times 10^8\, W/m^2$ [9, 16].

Figures 1 (a) and (b) present the confinement potential of the Deng-Fan type QW and the squared wave functions of the ground state electron for two different z_o, and L-values, respectively. Where L is the width parameter, z_o parameter reveals the asymmetric nature of the potential for $z > 0$. This asymmetry reflects a realistic heterostructure interface where interface roughness creates non-uniform barriers. Increasing parameter- z_o broadens the well and reduces the right-side barrier height while maintaining the left barrier. Increasing parameter- L for a constant z_o-value expands the confinement region. Squared wave function shows how the spatial extension of the electron within the well changes depending on external parameters. Furthermore, for both also parameters, the barrier height on the left remains unaffected while it begins to widen to the left. These tunable characteristics of the Deng-Fan potential independent

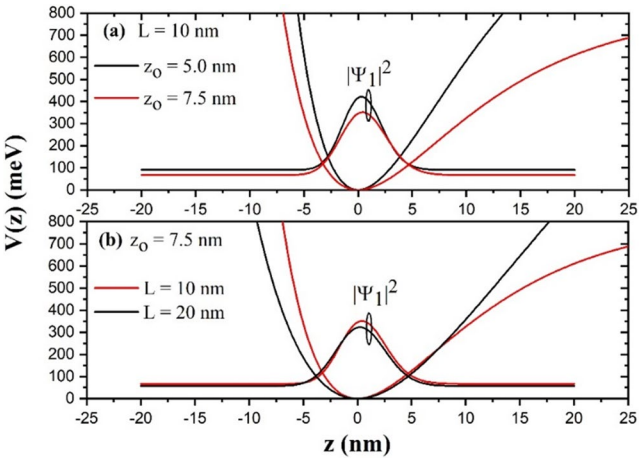


Fig. 1 (**a**, **b**) The z-dependent Deng-Fan type confinement potential profile and the ground state probability density of the electron for $L = 10\, nm$ and two different z_o values ($z_o = 5.0\, nm$ and $z_o = 7.5\, nm$) (a), for a constant $z_o (= 7.5\, nm)$ and two different L values ($L = 10\, nm$ and $L = 20\, nm$) (b). The energy axis value of the wave functions) (a), and for two different L values (b). The energy axis value of the wave functions shows the energy of the relevant level

control of confinement strength via L and asymmetry via z_o make it particularly important for modeling realistic QW structures.

3.1 Magnetic field effects

For $z_o = 5.0\, nm$, in the absence and presence of the magnetic field the variations of the two lowest energy values and also the energy difference between these levels corresponding to the confined electron in the Deng-Fan QW versus the well width, and the total absorption peaks corresponding to the (1–2) transition versus the incident photon energy for four different well widths are given in Figs. 2 (a) and (b), respectively. It should be noted that In Fig. 2(b), results are given only for $B = 0.0$ and $B = 15\, T$ to avoid mixing of absorption peaks. As illustrated in Fig. 2(a), an increase in the QW width leads to a decrease in both the energy levels and the energy difference between the two specified lowest states as quantum confinement weakens with increasing well width. The application of a magnetic field provides an additional parabolic confinement and leads to an increase in both energy levels due to the quantization of in-plane of the electron motion. Notably, the magnetic field effect is much weaker than that of geometric confinement. Figure 2 (b) shows the total absorption peaks corresponding to the (1–2) transition as a function of the incident photon energy for different width values. The total absorption peak positions directly mirror the energy difference changes relative to the well width- L as shown in Fig. 2 (a). An increase in L is seen to cause a red shift spanning the mid-infrared to far-infrared range. This tunability is crucial for designing wavelength-specific infrared detectors.

Absorption peaks exhibit the blue shift with increasing magnetic field, corresponding to the magnetic-field-induced enhancement in the intersubband energy difference. However, the magnitude of this shift is significantly smaller than that caused by variations in the well width, reinforcing the conclusion that structural parameters play the dominant role in determining the optical response of the Deng–Fan QW. For clarity, the results corresponding to $B = 10\, T$ are omitted in Fig. 2 (b).

Figures 3 (a) and (b) exhibit the same trends as Figs. 2 (a) and (b), but it is for $z_o = 7.5\, nm$. While the qualitative trends remain consistent with Fig. 2 (a, b), all spectral features appear at lower energies. The absorption spectrum, which shows peaks shifted further towards red compared to Fig. 2 (b), indicates a decrease in confinement strength. Since the increase in the parameter- z_o causes the geometric confinement to weaken, the energy difference is reduced and thus the positions of the total absorption peaks corresponding to the (1–2) transition are located at lower photon energies. In this context, parameter- z_o can be defined

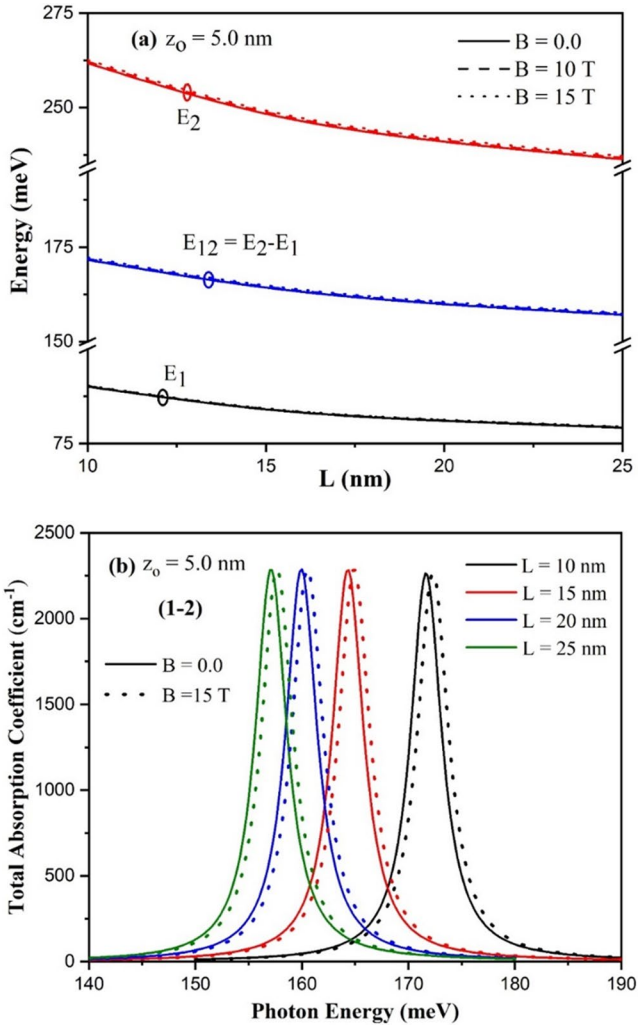


Fig. 2 (**a**, **b**) For $z_o = 5.0\,nm$, in the absence and presence of the magnetic field the variations of the two lowest energy values and also the energy difference between these levels corresponding to the confined electron in the Deng-Fan QW versus the well width (a), and the total absorption peaks corresponding to the (1–2) transition versus the incident photon energy for four different well widths, and only $B = 15\,T$ (b). The results are for $B = 0.0$ (solid lines), $B = 10\,T$ (dashed lines) and $B = 15\,T$ (dotted lines). The inset of the figure indicates which color corresponds to which well width

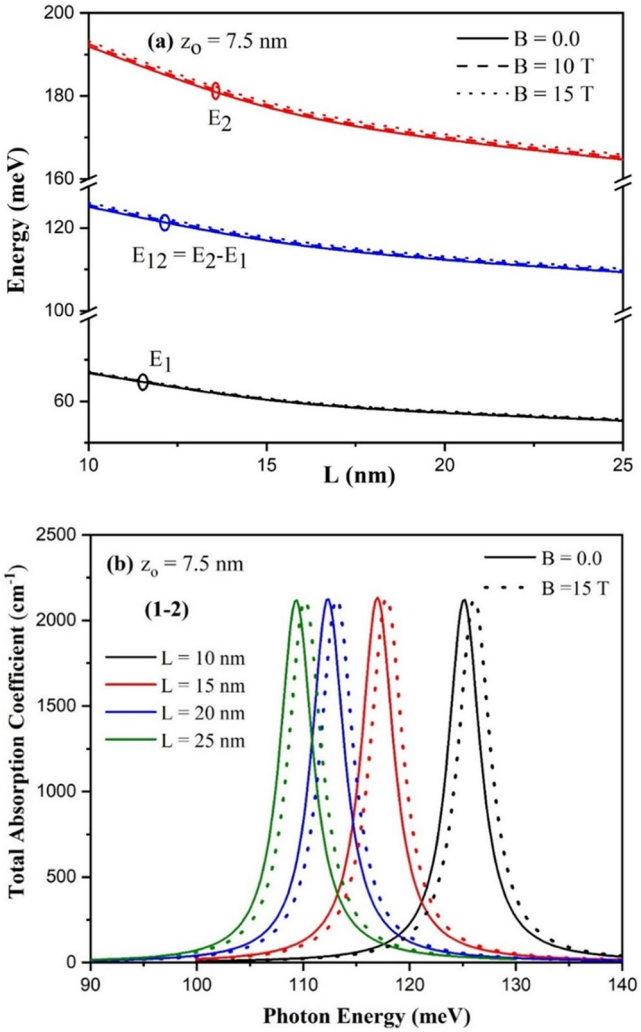


Fig. 3 (**a**, **b**) For $z_o = 7.5\,nm$, in the absence and presence of the magnetic field the variations of the two lowest energy values and also the energy difference between these levels corresponding to the confined electron in the Deng-Fan QW versus the well width (a), and the total absorption peaks corresponding to the (1–2) transition versus the incident photon energy for four different well widths, and only $B = 15\,T$ (b). The results are for $B = 0.0$ (solid lines), $B = 10\,T$ (dashed lines) and $B = 15\,T$ (dotted lines). The inset of the figure indicates which color corresponds to which well width

as a structural tuning parameter, allowing the absorption peaks to be shifted toward the red or blue of the spectrum as needed. This adjustability enables the fine-tuning of the material's optical properties, facilitating applications in fields such as photonics and sensor technology. By carefully selecting structural parameters, researchers can achieve desired electronic and optical responses, thereby enhancing device functionality. Such an advanced approach allows for the development of highly specialized materials tailored for specific applications, ranging from improved light absorption in solar cells to enhanced detection sensitivity in chemical sensors.

3.2 Pressure effects

It should be noted that the parameters L and z_o, which are defined in the absence of pressure in the figures, are given as $L(0)$ and $z_o(0)$ when the effect of pressure is taken into account.

Figure 4 (a, b) follows the same layout as Fig. 2 (a, b), but here the effects of the pressure are investigated. The energies, and the energy difference between the two considered energy levels are decreasing functions of the well dimensions and increasing functions of the pressure. The pressure has a greater effect on the energies than the magnetic

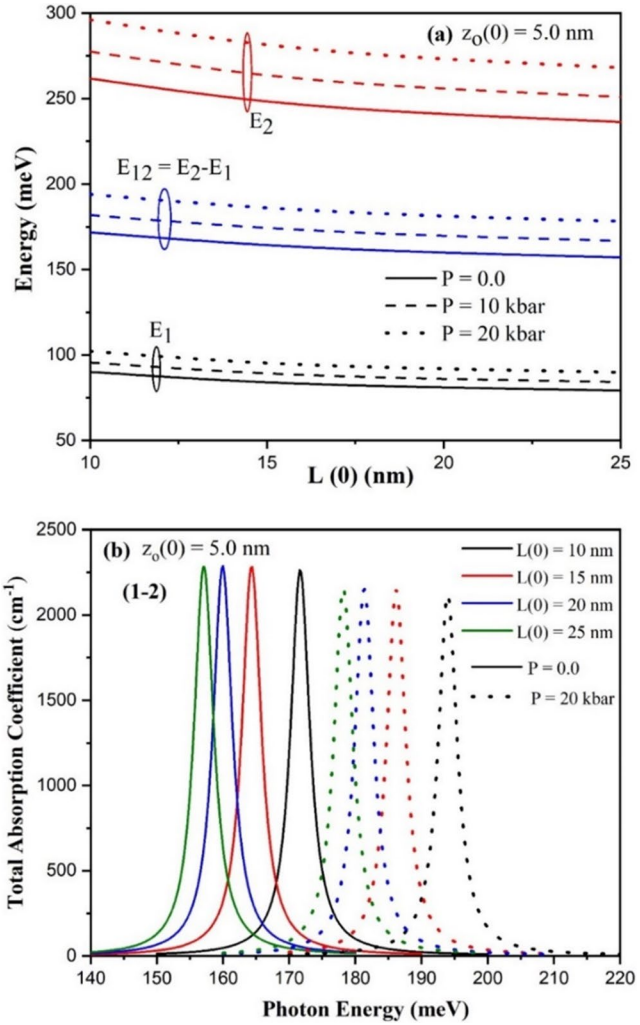


Fig. 4 (**a**, **b**) For $z_o\,(0) = 5.0\,nm$, the variations of the two lowest energy values and also the energy difference between these levels corresponding to the confined electron in the Deng-Fan QW versus the well width for $P = 0.0$ (solid lines), $P = 10\ kbar$ (dashed lines) and $P = 20\ kbar$ (dotted lines) (a), and the total absorption peaks corresponding to the (1–2) transition as a function of the incident photon energy for different well widths and pressure values ($P = 0.0$ (solid lines), $P = 20\ kbar$ (dotted lines)) (b)

field. As a result, a strong blue shift is observed in the total absorption peaks of the (1–2) transition due to the increase in the energy difference. The amount of shift in the peaks is approximately 23 meV for each $L\,(0)$ value. To illustrate the reasons for the behaviors indicated is given in Fig. 5 (a-d). In Fig. 5 (a-d), the variations of the effective mass, dielectric constant, the well width and the potential height are shown as a function of the pressure, respectively. As seen in these figures, the effective mass of the electron and the depth of the QW in which it is confined increase with pressure, while the dielectric constant and the width of the QW decrease. The combined effects of these four parameters produce the strong pressure response. This multi-parameter tunability makes hydrostatic pressure a uniquely powerful experimental probe for systematically modifying quantum well properties. Since the narrowing of the wells creates a strong confinement, a strong blue shift is observed in the absorption peaks due to the increase in energies and the energy difference. This blue shift indicates a change in the optical properties of the QW, which can have significant implications for the design of optoelectronic devices. As the confinement becomes stronger, the transition energies become more pronounced, enhancing the performance of applications such as lasers and photodetectors [30].

The magnetic field preserves peak amplitudes (as shown Figs. 2 (b) and 3 (b)) since it does not significantly alter the spatial distributions of the wave function. In contrast, hydrostatic pressure fundamentally reshapes the wave functions by physically compressing the structure and modifying material parameters, thereby affecting both the transition energies and strengths.

Figure 6 (a, b) exhibit the same trend as Fig. 4 (a, b), but it is for $z_o\,(0) = 7.5\,nm$. The pressure dependence of the energies, and also the energy differences between the relevant energy levels, and the changes in the positions of the absorption peaks are similar to those shown in Figs. 5 (a) and (b). However, since the increase in parameter- z_o causes a weakening of the geometric confinement, the values of these specified parameters for $z_o\,(0) = 7.5\,nm$ are lower than those for $z_o\,(0) = 5.0\,nm$ and consequently, the absorption peaks are located at lower photon energies.

As known, the dipole matrix element- M_{ij} reflects the strength of the light absorption. The change in the positions of the absorption peaks depends directly on the energy difference between the two considered energy levels, whereas the peak amplitudes depend on both this energy difference and the dipole matrix element. Consequently, an understanding of the overall absorption characteristics of the system requires knowledge of both the energy difference and the dipole matrix element. Therefore, in order to explain the changes in absorption peak amplitudes, the variations of squared reduced dipole matrix elements (RDME represents the ratio of the dipole matrix element to the electron charge) as a function of the well width are given in Figs. 7 (a) and (b) for $z_o\,(0) = 5.0\,nm$ and $z_o\,(0) = 7.5\,nm$, respectively. The reason for defining RDME- $\eta_{ij}\,(= \frac{M_{ij}}{e})$ is to express it in length units. Since the Deng-Fan potential has an asymmetric character, Figs. 7 (a) and (b) contain both diagonal and non-diagonal squared RDMEs. As seen in Figs. 2 (b) and 3(b), the well width and magnetic field have almost no effects on the amplitude of the absorption peaks in contrast, the effect of pressure on the peak amplitudes is more evident as seen in Figs. 4 (b) and 6 (b). Pressure causes a decrease in the peak amplitudes. As seen in Eqs. (13) and (14), the linear absorption coefficient depends on $|M_{ij}|^2$ term, while

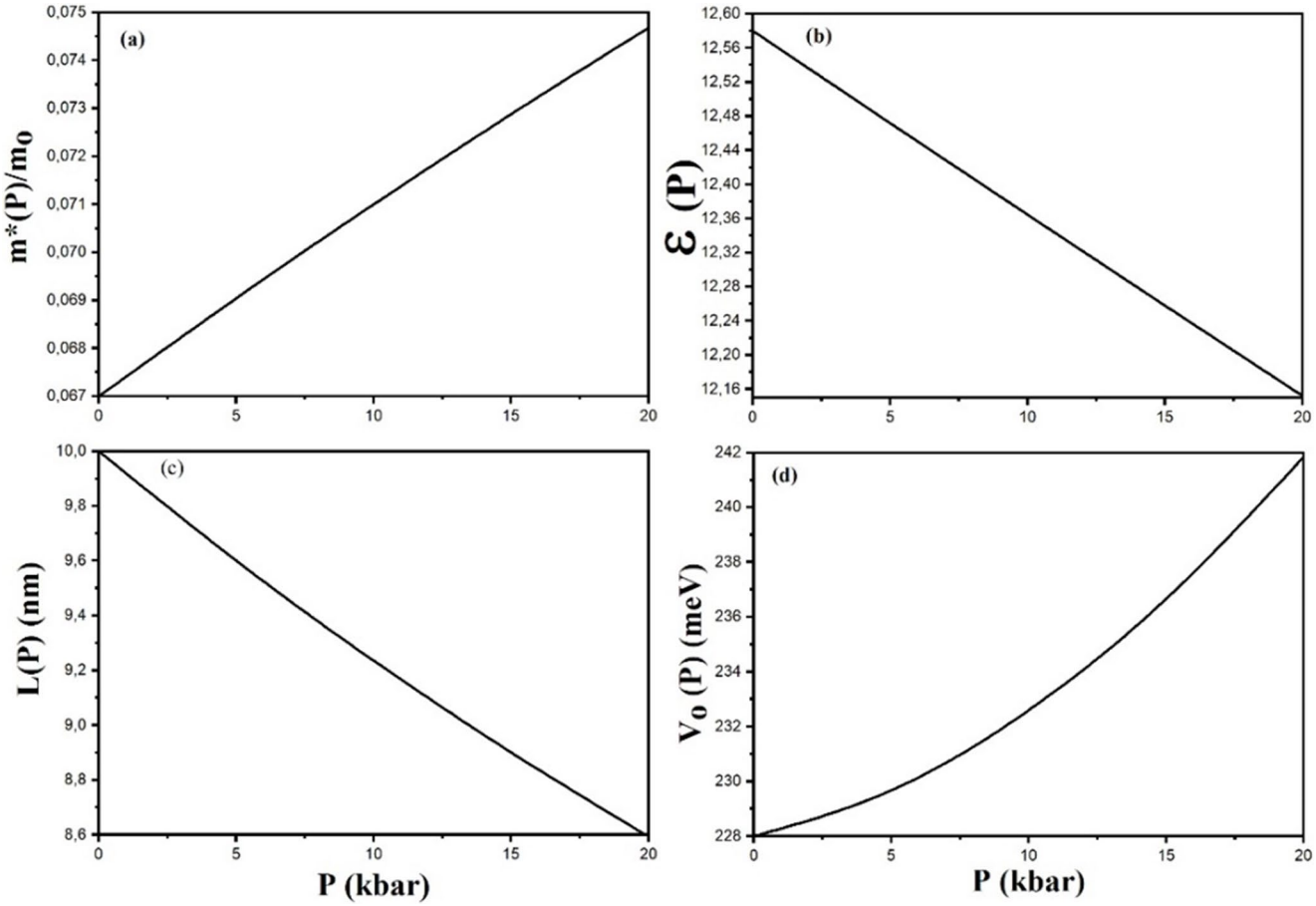


Fig. 5 (**a-d**) The variations of the effective mass, dielectric constant, the well width and the potential height as a function of the pressure, respectively

the nonlinear absorption coefficient depends on the $|M_{ij}|^4$ and $|M_{22} - M_{11}|^2$ terms. Since these terms decrease under the influence of pressure, the amplitudes of the absorption peaks also decrease as pressure increases.

3.3 A comparison of Morse and Deng-Fan potentials

To compare the Deng-Fan potential with the modified Morse potential [31], comparative calculations were performed using the same material parameters (GaAs) The Morse potential is given as follows,

$$V(z) = V_0\left(1 - e^{-z/L)}\right)^2 \tag{17}$$

It should be noted that, all parameters in this equation are defined before. The Morse and Deng-Fan potential profiles are compared in Figs. 8 (a) and (b) for two different values of the asymmetry parameter ($z_o = 5.0\,nm$ and $z_o = 10\,nm$), which is absent in the Morse potential but present in the Deng-Fan potential, and for a single L-value ($L = 10\,nm$). As seen in these figures, while the potentials coincide at the equilibrium position, the Deng-Fan potential exhibits a steeper repulsive branch compared to the relatively flatter the Morse potential. The steeper repulsive branch causes the wave function to be confined to a narrower area. Strong confinement creates an increase in momentum and therefore kinetic energy, this means an increase in energy levels. Rong et al. [31] compared the Deng-Fan confinement potential with the Morse potential for several diatomic molecules, noting that while the Deng-Fan potential is qualitatively similar to the Morse model, it exhibits the correct asymptotic behavior as the internuclear distance approaches zero. Furthermore, they observed that for certain molecules, the Morse potential underestimates experimental results, whereas the Deng-Fan model provides more accurate predictions. Since an increase in the parameter- z_o causes an expansion of the QW and a decrease in the right-side barrier height, the structure begins to converge toward a Morse-type QW. To determine conditions under which the two potentials become fully compatible, Fig. 9 presents the variation of the ground-state energy of an electron in a Deng-Fan type QW with respect to the parameter- z_o for $L = 10\,nm$, alongside the energy in a Morse type QW of the same width

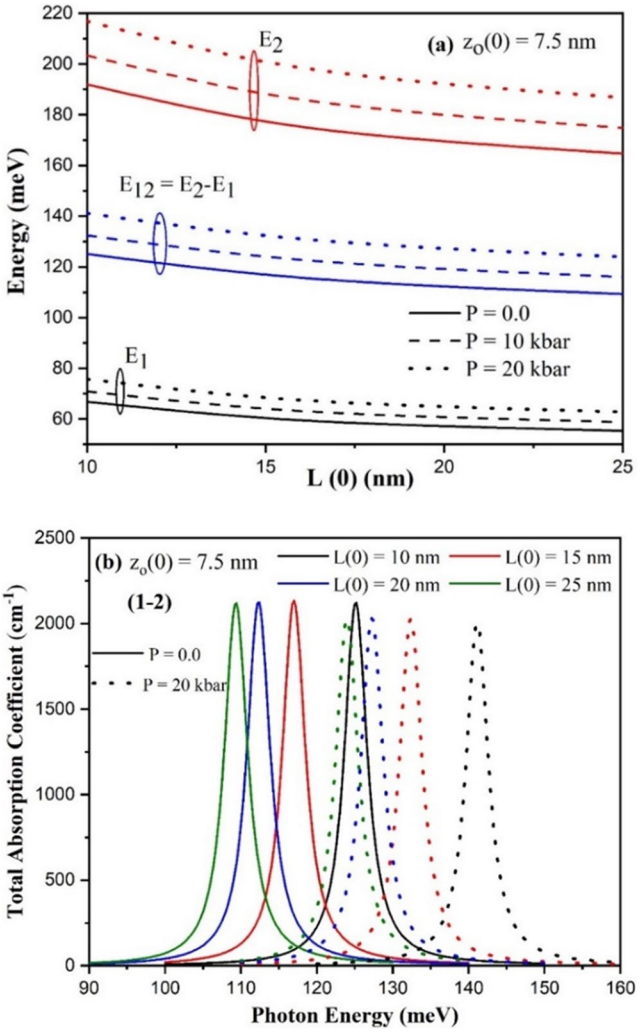


Fig. 6 (**a**, **b**) For $z_o\,(0) = 7.5\,nm$, the variations of the two lowest energy values and also the energy difference between these levels corresponding to the confined electron in the Deng-Fan QW versus the well width for P=0.0 (solid lines), P=10 kbar (dashed lines) and P=20 kbar (dotted lines) (a), and the total absorption peaks corresponding to the (1–2) transition as a function of the incident photon energy for different well widths and pressure values (P=0.0 (solid lines), P=20 kbar (dotted lines)) (b)

(it is important to remember that the result of the Morse QW is independent of the z_o parameter). As can be seen, with increasing asymmetry parameter in Deng-Fan type QW, the results increasingly coincide with those of Morse-type QW.

Figures 10(a) and (b) show the variations of E_1, E_2 and $E_{12} = E_2 - E_1$ as a function of the QW width for the Morse QW in the presence of the magnetic field (a), and the hydrostatic pressure (b), respectively. It is important to note that the symbols L and z_o used in the absence of pressure, are replaced by $L\,(P)$ and $z_o\,(P)$ when investigating the effects of pressure. The pressure-dependent expression of the Morse potential defined in Eq. (17) is as follows.

$$V\,(z,\,P) = V_0\,\,(P)\left(1 - e^{-z/L(P))}\right)^2 \tag{18}$$

It should be noted that the parameters used here have been defined previously.

As in the Deng-Fan QW, the energies E_1, E_2 and $E_{12} = E_2 - E_1$ are a decreasing function of the well width, whereas they are increasing functions with respect to the magnetic field and hydrostatic pressure. However, due to the weaker geometric confinement of the Morse QW, its energy levels are considerably lower.

The total absorption peaks corresponding to the (1–2) intraband transition for the electron confined in the Morse QW as a function of the incident photon energy for different well widths under the magnetic field, and the hydrostatic pressure are given in Figs. 11 (a) and (b), respectively. Regardless of the value of z_o-value used for the comparison, it is observed that the peak positions of the total absorption coefficients associated with the (1–2) intraband transitions in the Morse quantum well are located at relatively low photon energies, due to the small energy separation between the corresponding levels. In addition, the peak decrease as the dipole matrix elements (DME) increases. We did not provide the results of DME for Morse potential depending on external parameters here, as Fig. 9 demonstrates that the Deng-Fan QW results coincide with the Morse QW results as z_o increases. Accordingly, it is evident that there is an increase in DME for Morse QW, consistent with Fig. 7(a, b), since large z_o-values lead to an enhanced in DME and subsequent decrease in peak amplitudes. Ultimately, the Deng-Fan potential produces larger transition energies and higher peak amplitudes for equivalent widths while offering superior control over potential asymmetry.

4 Conclusion

This study investigates the effects of a magnetic field, hydrostatic pressure, and structural parameters on the energy spectrum and intraband transitions of an electron confined in a QW with a Deng-Fan potential, which has an asymmetric character. Our results show that the electronic and optical properties of the QW with Deng-Fan potential are highly sensitive to the sizes of the QW, whereas the influence of the magnetic field is relatively minor. To provide a comprehensive comparison, our calculations were extended to include the traditional Morse-type QW. A key finding is that while the asymmetry of the Morse potential remains constant, the Deng-Fan potential features an adjustable asymmetry parameter. This flexibility allows for better alignment with experimental data, making the Deng-Fan

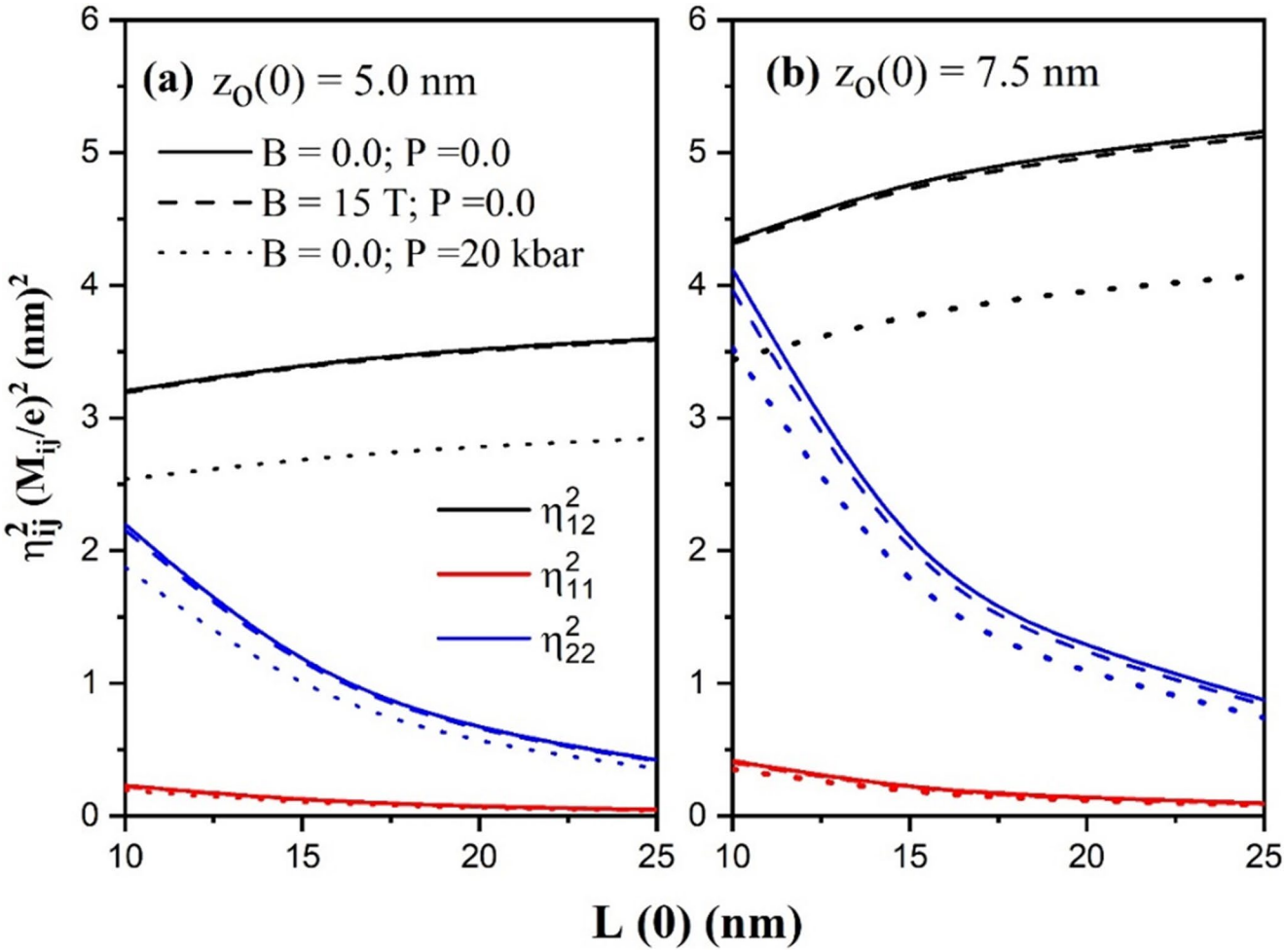


Fig. 7 The variations of the reduced dipole matrix elements versus the quantum well width in the absence and presence of the external probes for two different z_o-values: for $z_o\,(0) = 5.0\,nm$ (**a**), and $z_o\,(0) = 7.5\,nm$ (**b**), respectively

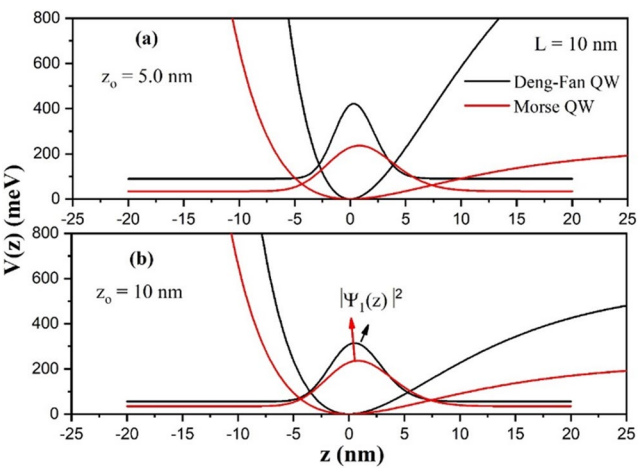


Fig. 8 (**a**, **b**) The Morse and Deng-Fan potential profiles for two values of the asymmetry parameter in the Deng-Fan potential and the ground state probability densities of the electron versus the z-coordinate: $z_o = 5.0\,nm$ (a), and $z_o = 10\,nm$ (b)

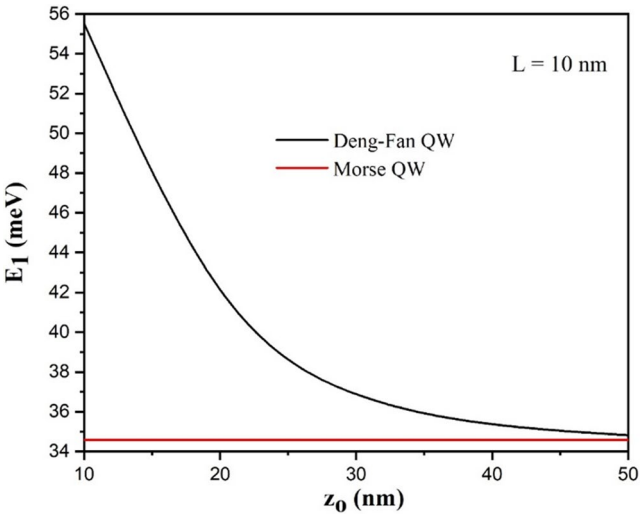


Fig. 9 For $L = 10\,nm$, the variation of the ground-state energy of an electron in a Deng-Fan type QW as a function of the parameter- z_o (black line), and electron energy in a Morse type QW of the same width (red line)

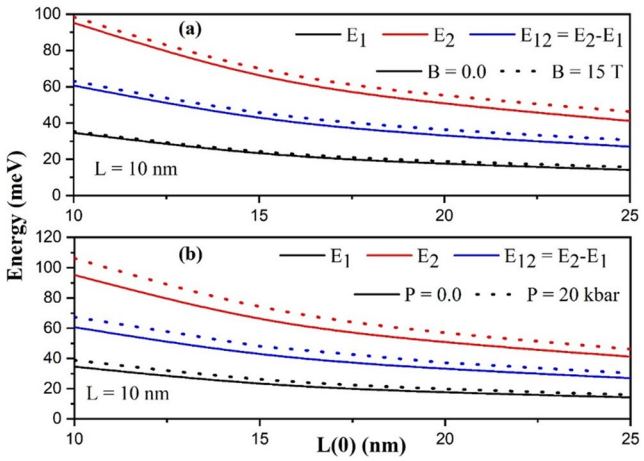


Fig. 10 (**a**, **b**) The two lowest energy values(E_1 and E_2) of the confined electron in the Morse QW, and the energy difference ($E_{12} = E_2 - E_1$) between these levels as a function of the width parameter in the presence of the magnetic field (a), and hydrostatic pressure (b). Solid (dotted) lines are for $B = 0.0 \,\&\, P = 0.0$ ($B = 15\,T \,\&\, P = 20\,kbar$)

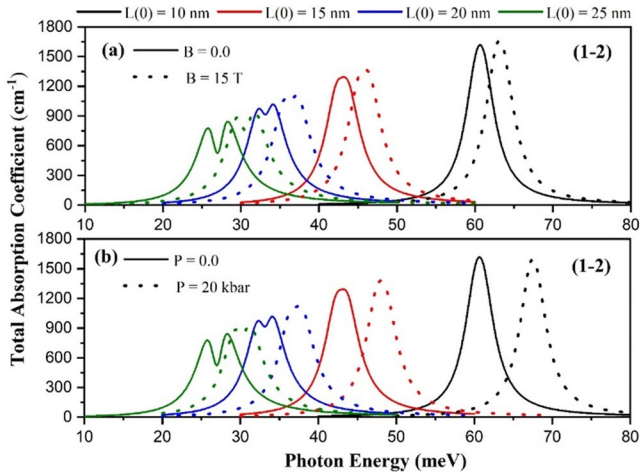


Fig. 11 (**a**, **b**) The total absorption peaks corresponding to the (1–2) intraband transition for the confined electron in the Morse QW as a function of the incident photon energy for different widths in the presence of the magnetic field (a), and hydrostatic pressure (b). Solid (dotted) lines are for $B = 0.0 \,\&\, P = 0.0$ ($B = 15\,T \,\&\, P = 20\,kbar$)

potential more advantageous and versatile than the Morse potential. Consequently, this potential model offers a promising framework for future studies in low-dimensional semiconductor physics.

Author contributions Esin Kasapoglu: Conceptualization, Methodology, Theoretical Modeling, Formal Analysis, Software Development, Visualization, Writing – Original Draft Preparation, Writing – Review & Editing. M. Behiye Yücel: Conceptualization, Methodology, Visualization, Writing – Review & Editing.

Funding Open access funding provided by the Scientific and Technological Research Council of Türkiye (TÜBİTAK). The authors did not receive support from any organization for the submitted work.

Data availability This manuscript has no associated data added to any data repository.

Declarations

Conflict of interests The authors declare no competing interests.

Open Access This article is licensed under a Creative Commons Attribution 4.0 International License, which permits use, sharing, adaptation, distribution and reproduction in any medium or format, as long as you give appropriate credit to the original author(s) and the source, provide a link to the Creative Commons licence, and indicate if changes were made. The images or other third party material in this article are included in the article's Creative Commons licence, unless indicated otherwise in a credit line to the material. If material is not included in the article's Creative Commons licence and your intended use is not permitted by statutory regulation or exceeds the permitted use, you will need to obtain permission directly from the copyright holder. To view a copy of this licence, visit http://creativecommons.org/licenses/by/4.0/.

References

1. Xie Wen-Fang, Two interacting electrons in a spherical Gaussian confining potential quantum well. Commun. Theor. Phys. **42**, 151–154 (2004). https://doi.org/10.1088/0253-6102/42/1/151
2. M.G. Barseghyan, A.A. Kirakosyan, Electronic states in a step quantum well in a magnetic field. Phys. E. **28**, 471–481 (2005). https://doi.org/10.1016/j.physe.2005.05.058
3. J.A. Gil-Corrales, A.L. Morales, C.A. Duque, Self-consistent study of GaAs/AlGaAs quantum wells with modulated doping. Nanomaterials. **13**, 913 (2023). https://doi.org/10.3390/nano13050913
4. M. Solaimani, I. Morteza, H. Arabshahi, S.M. Reza, Effect of the magnetic field on optical properties of GaN/AlN multiple quantum wells. J. Lumin. **134**, 88–95 (2013). https://doi.org/10.1016/j.jlumin.2012.09.007
5. Z.H. Zhang, L. Zou, K.-X. Guo, J.H. Yuan, The nonlinear optical rectification in asymmetrical and symmetrical Gaussian potential quantum wells with applied electric field. Opt. Commun. **359**, 316–321 (2016). https://doi.org/10.1016/j.optcom.2015.10.015
6. H. Sari, F. Ungan, E. Kasapoglu, S. Sakiroglu, I. Sökmen, Intense laser-induced electronic and optical properties in double finite oscillator potential. Phil Mag. **99**, 2444–2456 (2019). https://doi.org/10.1080/14786435.2019.1617907
7. S. Baskoutas, C. Garoufalis, A.F. Terzis, Linear and nonlinear optical absorption coefficients in inverse parabolic quantum wells under static external electric field. Eur. Phys. J. B **84**, 241–247 (2011). https://doi.org/10.1140/epjb/e2011-20470-9
8. A. AL-Naghmaish, H. Dakhlaoui, T. Ghrib, B.M. Wong, Effects of magnetic, electric, and intense laser fields on the optical properties of AlGaAs/GaAs quantum wells for terahertz photodetectors. Phys. B **635**, 413838 (2022). https://doi.org/10.1016/j.physb.2022.413838
9. A. Shaer, M.B. Yücel, E. Kasapoglu, Hydrostatic pressure and temperature dependent optical properties of double inverse parabolic quantum well under the magnetic field. Phys. B **685**, 416057 (2024). https://doi.org/10.1016/j.physb.2024.416057
10. N. Yahyaoui, K. Hammouda, N. Zeiri, M. Said, M.E. El Sayed Ali, A. Samir Aly Hendi, C.A. Duque, Impact of the applied electric field on the optical absorption coefficient in Ge/$Si_{1-x}Ge_x$ step quantum well (SQW). Discov Appl. Sci. **7**, 403 (2025). https://doi.org/10.1007/s42452-025-06685-z

11. Z.-H. Zhang, J.-H. Yuan, K.-X. Guo, The Combined Influence of Hydrostatic Pressure and Temperature on Nonlinear Optical Properties of GaAs/$Ga_{0.7}Al_{0.3}$As Morse Quantum Well in the Presence of an Applied Magnetic Field. Materials. **11**, 668–677 (2018). https://doi.org/10.3390/ma11050668
12. H. Azmi, K. El-Bakkari, A. Fakkahi, A. Mazouz, M. Jaouane, A. Ed-Dahmouny, R. Arraoui, M. Jaafar, A. Sali, N. Amri, El Ghazi, Magnetic impurity-related optical absorption coefficients in a semimagnetic double quantum well under magnetic field and temperature effects. Appl. Phys. A **131**, 424 (2025). https://doi.org/10.1007/s00339-025-08551-6
13. Z.-H. Zhang, J.-H. Yuan, K.-X. Guo, The combined influence of hydrostatic pressure and temperature on nonlinear optical properties of GaAs/$Ga_{0.7}Al_{0.3}$As Morse Quantum well in the presence of an applied magnetic field. Materials **11**, 668 (2018). https://doi.org/10.3390/ma11050668
14. O.I. Olusola, O.P. Shomotun, U.E. Vincent, P.V.E. McClintock, Quantum vibrational resonance in a dual-frequency-driven Tietz-Hua quantum well. Phys. Rev. E. **101**, 052216 (2020). https://doi.org/10.1103/PhysRevE.101.052216
15. K.A. Rodríguez-Magdaleno, F.M. Nava-Maldonado, E. Kasapoglu, M.E. Mora-Ramos, F. Ungan, Martínez-Orozco, Nonlinear absorption coefficient and relative refractive index change for Konwent potential quantum well as a function of intense laser field effect. Phys. E. **148**, 115618 (2023). https://doi.org/10.1016/j.physe.2022.115618
16. E. Kasapoglu, C.A. Duque, The effects of external fields on double GaAs/AlGaAs quantum well with Manning potential. Mater. Sci. Semiconduct. Process. **137**, 106232 (2022). https://doi.org/10.1016/j.mssp.2021.106232
17. F. Ungan, M.K. Bahar, The laser field controlling on the nonlinear optical specifications of the electric field-triggered Rosen-Morse quantum well. Phys. Lett. A **384**, 126400 (2020). https://doi.org/10.1016/j.physleta.2020.126400
18. E. Kasapoglu, H. Sari, I. Sökmen, J.A. Vinasco, D. Laroze, C.A. Duque, Effects of intense laser field and position dependent effective mass in Razavy quantum wells and quantum dots. Phys. E. **126**, 114461 (2021). https://doi.org/10.1016/j.physe.2020.114461
19. M. Gambhir, B. Vidhani, S. Devi, V. Prasad, Impact of asymmetry of Razavy-type coupled well system and static electric field on the time-dynamical studies of entanglement. Eur. Phys. J. Plus. **138**, 57–68 (2023). https://doi.org/10.1140/epjp/s13360-023-03683-1
20. Z.H. Deng, Y.P. Fan, A potential function of diatomic molecules. J. Shandong Univ. J. **7**, 162 (1957). (Natural Science)
21. X. Ceng Chang, X. Li, C. Wang, Zhang, Nonlinear optical properties in GaAs/Ga0.7Al0.3As spherical quantum dots with Like-Deng-Fan-Eckart potential. Phys. Lett. A **467**, 128732 (2023). https://doi.org/10.1016/j.physleta.2023.128732
22. X. Li, Y. Duan, Third-harmonic generation in spherical quantum dots under Deng–Fan–Eckart potential: Effects of hydrostatic pressure, temperature and Al-concentration. Phys. E. **144**, 115453 (2022). https://doi.org/10.1016/j.physe.2022.115453
23. C.O. Edet, U.S. Okorie, G. Osobonye, A.N. Ikot, G.J. Rampho, R. Sever, Thermal properties of Deng–Fan–Eckart potential model using Poisson summation approach. J. Math. Chem. **58**, 989–1013 (2020). https://doi.org/10.1007/s10910-020-01107-4
24. E. Kasapoglu, The effects of the magnetic and non-resonant intense laser fields on the electronic and optical properties of the shifted Deng–Fan type quantum well. Opt. Quant. Electron. **57**, 585 (2025). https://doi.org/10.1007/s11082-025-08509-1
25. E. Kasapoglu, Hydrostatic pressure effects on the electronic and optical properties of isotropic and anisotropic 2D quantum dots with the Deng-Fan oscillator potential. Indian J. Phys. (2026). https://doi.org/10.1007/s12648-025-03907-3
26. H. Dakhlaoui, J.A. Gil-Corrales, A.L. Morales, E. Kasapoglu, A. Radu, R.L. Restrepo, V. Tulupenko, J.A. Vinasco, M.E. Mora-Ramos, C.A. Duque, Theoretical study of electronic and optical properties in doped quantum structures with Razavy confining potential: effects of external fields. J. Comput. Electron. **21**, 378–395 (2022). https://doi.org/10.1007/s10825-022-01859-z
27. H.J. Ehrenreich, Band Structure and Transport Properties of Some 3–5 Compounds. J. Appl. Phys. **32**, 2155–2166 (1961). https://doi.org/10.1063/1.1777035
28. D.E. Aspnes, GaAs lower conduction-band minima: Ordering and properties. Phys. Rev. B **14**, 5331–5343 (1976). https://doi.org/10.1103/PhysRevB.14.5331
29. S. Adachi, GaAs, AlAs, and $Al_xGa_{1-x}As$: Material parameters for use in research and device applications. J. Appl. Phys. **58**, R1–R29 (1985). https://doi.org/10.1063/1.336070
30. R.F. Kopf, M.H. Herman, M.L. Schnoes, A.P. Perley, G. Livescu, M. Ohring, Band offset determination in analog graded parabolic and triangular quantum wells of GaAs/AlGaAs and GaInAs/AlInAs. J. Appl. Phys. **71**, 5004–5011 (1992). https://doi.org/10.1063/1.350600
31. Z. Rong, H.G. Kjaergaard, M.L. Sage, Comparison of the Morse and Deng-Fan potentials for X-H bonds in small molecules. Mol. Phys. **101**, 2285–2294 (2003). https://doi.org/10.1080/00268970310001377706

Publisher's note Springer Nature remains neutral with regard to jurisdictional claims in published maps and institutional affiliations.